Implications of Non-cylindrical Flux Ropes for Magnetic Cloud Reconstruction Techniques and the Interpretation of Double Flux Rope Events

M.J. Owens · P. Démoulin · N.P. Savani · B. Lavraud · A. Ruffenach

Abstract Magnetic clouds (MCs) are a subset of interplanetary coronal mass ejections (ICMEs) which exhibit signatures consistent with a magnetic flux rope structure. Techniques for reconstructing flux rope orientation from single-point *in situ* observations typically assume the flux rope is locally cylindrical, *e.g.*, minimum variance analysis (MVA) and force-free flux rope (FFFR) fitting. In this study, we outline a non-cylindrical magnetic flux rope model, in which the flux rope radius and axial curvature can both vary along the length of the axis. This model is not necessarily intended to represent the global structure of MCs, but it can be used to quantify the error in MC reconstruction resulting from the cylindrical approximation. When the local flux rope axis is approximately perpendicular to the heliocentric radial direction, which is also the effective spacecraft trajectory through a magnetic cloud, the error in using cylindrical reconstruction methods is relatively small ($\approx 10°$). However, as the local axis orientation becomes increasingly aligned with the radial direction, the spacecraft trajectory may pass close to the axis at two separate locations. This results in

M.J. Owens (✉)
Space Environment Physics Group, Department of Meteorology, University of Reading, Earley Gate, PO Box 243, Reading RG6 6BB, UK
e-mail: m.j.owens@reading.ac.uk

M.J. Owens
Space and Atmospheric Physics, Imperial College London, Prince Consort Road, London SW7 2AZ, UK

P. Démoulin
Observatoire de Paris, Section de Meudon, 92195 Meudon Cedex, France

N.P. Savani
Solar-Terrestrial Environment Laboratory, Nagoya University, Nagoya, Japan

B. Lavraud · A. Ruffenach
Institut de Recherche en Astrophysique et Planétologie (IRAP), Université de Toulouse (UPS), Toulouse, France

B. Lavraud · A. Ruffenach
Centre National de la Recherche Scientifique, UMR 5277, Toulouse, France

a magnetic field time series which deviates significantly from encounters with a force-free flux rope, and consequently the error in the axis orientation derived from cylindrical reconstructions can be as much as 90°. Such two-axis encounters can result in an apparent 'double flux rope' signature in the magnetic field time series, sometimes observed in spacecraft data. Analysing each axis encounter independently produces reasonably accurate axis orientations with MVA, but larger errors with FFFR fitting.

Keywords Magnetic cloud · Magnetic flux rope · Coronal mass ejection · Solar wind

1. Introduction

The interplanetary manifestations of coronal mass ejections, ICMEs (see *e.g.*, Wimmer-Schweingruber *et al.*, 2006 and references therein), drive the largest disturbances to the geomagnetic magnetic field (*e.g.*, Gosling, 1993; Cane and Richardson, 2003). The geo-effectiveness of an ICME is primarily determined by the relative orientation of the ICME (*e.g.*, Lavraud and Borovsky, 2008) and the terrestrial magnetic fields (Dungey, 1961). This is the product of an ICME's intrinsic properties and its orientation and position relative to the terrestrial system. Aside from space weather concerns, ICME orientation is also a key parameter for a wide range of solar and heliospheric studies, such as associating ICMEs with their solar source regions (Wang *et al.*, 2006), the magnetic helicity carried by CMEs over the solar cycle (Lynch *et al.*, 2005), and their role in open flux transport at the Sun (Owens *et al.*, 2007; Lavraud, Owens, and Rouillard, 2011).

Magnetic clouds (MCs) are a subset of ICMEs predominantly characterised by a large-scale, smooth rotation in the magnetic field direction (Burlaga *et al.*, 1981; Klein and Burlaga, 1982). This signature has been interpreted and modelled as a magnetic flux rope (Burlaga, 1988; Lepping, Jones, and Burlaga, 1990), enabling reconstruction of the large-scale properties from single-point *in situ* observations, which essentially constitute a single radial cut through an ICME as it passes over a stationary spacecraft. By far the most commonly used form of flux rope model is the force-free flux rope (FFFR), which assumes that the current density is proportional to the magnetic field with a uniform constant and that locally the flux rope has the geometry of a cylinder with a circular cross section (Burlaga, 1988). Assuming a flux rope topology, minimum variance analysis (MVA; Sonnerup and Cahill, 1967) is able to quickly determine the axis orientation. This approach has proved immensely useful in interpreting MC observations, particularly the local axis orientation (*e.g.*, Bothmer and Schwenn, 1998). However, the circular cross section approximation is unlikely to be valid (Russell and Mulligan, 2002; Riley *et al.*, 2004; Owens and Cargill, 2004; Savani *et al.*, 2010). While this may not significantly affect estimates of axis orientation, particularly when the spacecraft encounters the axis (Owens, 2008), it has led researchers to incorporate cross-sectional elongation in the non-radial direction into the analytical models (*e.g.*, Hu and Sonnerup, 2001; Mulligan and Russell, 2001; Hidalgo *et al.*, 2002; Vandas and Romashets, 2003; Owens, Merkin, and Riley, 2006). Even in these more sophisticated models, the flux rope is usually still cylindrical (*i.e.*, the field is invariant with translation along the axis).

Evidence for non-cylindrical flux ropes in MCs stems from a number of sources. Coronagraph images of CMEs typically show both a curved leading edge and a curved dark cavity (Hundhausen, 1993), which has been interpreted as viewing curved flux rope axes lying in the plane of the sky (Cremades and Bothmer, 2004). In interplanetary space, MVA and FFFR reconstructions find MC flux ropes with a variety of orientations to the heliocentric radial

direction. When multiple, well-separated spacecraft observations of the same flux rope are available, the global structure is generally inferred to be a flux rope with a curved axial magnetic field (Burlaga *et al.*, 1981). Finally, counterstreaming suprathermal electrons (CSEs) are often associated with MCs and interpreted as evidence of 'closed' field lines which have both ends rooted at the photosphere (Gosling *et al.*, 1987). Thus ICME fields must form loops in the heliosphere, although the flux rope structure may not be present over the whole length of these loops (Yamamoto, Kataoka, and Inoue, 2010).

Efforts have been made to move away from the cylindrical approximation, most notably by assuming toroidal or spheromak geometry, wherein the axial field forms a closed ring in interplanetary space (see *e.g.*, Vandas, Fischer, and Geranios, 1991; Farrugia, Osherovich, and Burlaga, 1995; Marubashi and Lepping, 2007; Romashets and Vandas, 2009). Spacecraft trajectories through such structures frequently result in two encounters with the axial field (Vandas *et al.*, 1998), which may explain the ICMEs with a 'double flux rope' signature that are sometimes observed (Rees and Forsyth, 2004). Even though such models cannot be correct in a global sense, as the magnetic field within such a structure maintains no connection to the Sun, contrary to suprathermal electron observations (Gosling *et al.*, 1987), they are extremely useful for estimating the effect of local axial curvature.

We take a similar approach in this study and attempt to further quantify the error in the estimation of magnetic flux rope orientation which results from assuming cylindrical symmetry. This is achieved by generating synthetic spacecraft encounters with a curved flux rope (CFR) model, in which the axial curvature and cross-sectional extent can vary along the axis, as described in Section 2. Much like spheromak and toroidal models, we acknowledge that our model may not be a realistic representation of the global structure of MCs, but can provide a reasonable representation of local flux rope structure, necessary for our testing purposes. In Section 3, the time series generated with the CFR model is fit with cylindrical techniques, and the error in the axis orientation is calculated.

2. Curved Flux Rope (CFR) Model

In this section we outline an analytical flux rope model with a curved axial magnetic field. Currently, there is great uncertainty in the cross-sectional shape and non-radial extent of flux ropes in MCs (see *e.g.*, Russell and Mulligan, 2002; Hidalgo *et al.*, 2002; Hu and Sonnerup, 2001; Riley and Crooker, 2004), but spacecraft trajectories which pass close to the flux rope axis are largely unaffected by such different cross-sectional topologies (Riley *et al.*, 2004; Owens, 2008). For this reason, we assume a circular flux rope cross section, but limit all spacecraft trajectories to the plane containing the axial field. A suitably curved flux rope geometry can therefore be achieved by 'bending' an FFFR model. For simplicity, in this paper, we choose to bend the axial field in a similar manner to a Parker spiral magnetic field. This allows the radius of curvature of the axis and the cross-sectional extent of the flux rope to vary along the length of the axis. This geometry was recently used to estimate the length of field lines within MCs (Owens, Crooker, and Horbury, 2009), but here it is developed into a magnetic flux rope model. By taking various different spacecraft trajectories through the curved flux rope, we can approximate spacecraft encounters with flux ropes with a range of axis orientations.

Working in cylindrical polar coordinates $(\widehat{\mathbf{R}}, \widehat{\theta}, \widehat{\mathbf{Z}})$ in a fixed heliocentric frame with $\widehat{\mathbf{Z}}$ pointing along the solar rotation axis, and assuming that the bulk motion of the MC is radial at a solar wind speed V_{SW}, a section of the axis which left the Sun at time t previously will therefore be at position $\mathbf{P}_{\mathrm{A}}(t)$:

$$\mathbf{P}_{\mathrm{A}}(t) = V_{\mathrm{SW}}t\widehat{\mathbf{R}} + \Omega R t\widehat{\theta}, \tag{1}$$

Figure 1 The curved magnetic flux rope model used in this study. While we do not expect magnetic clouds (MCs) to have this global configuration, particularly to have axes aligned with the Parker spiral, it is a useful construct to investigate local morphology. The top panel shows the three-dimensional structure, with black, green, blue and red showing magnetic field lines at a normalised distance from the axis of $r = 0$, 0.3, 0.6 and 0.9, respectively. The bottom panel shows the projection onto the solar rotation (*i.e.*, $R-\theta$) plane. The black dashed lines indicate the front and rear boundaries of the flux rope, as defined by $r = 1$.
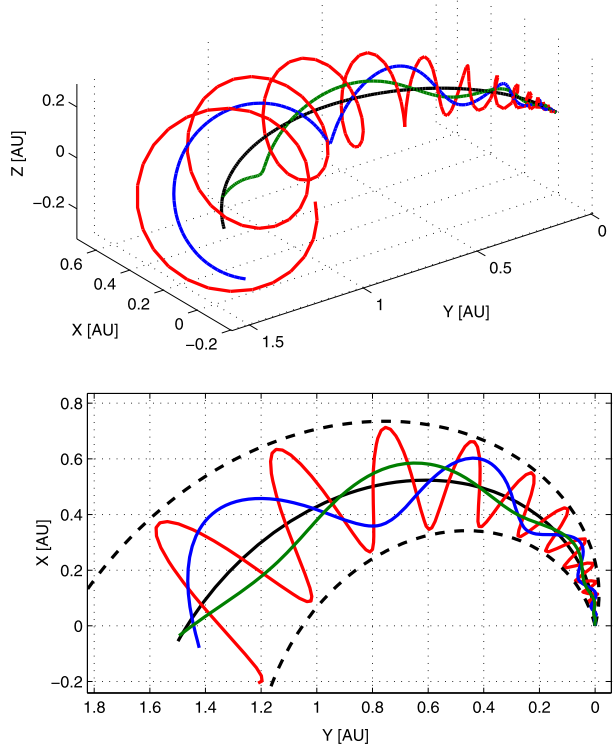
where R is the heliocentric distance, and Ω is the angular rotation speed of the Sun. This is shown as the solid black line in Figure 1. Note that we have selected a $+$ sign in front of Ω in Equation (1), the opposite sign of the Parker spiral, because we describe here the axis shape of a flux rope, not the interplanetary magnetic field. The $+$ sign in front of Ω describes the eastern leg of a flux rope coming to Earth, while the $-$ sign would describe the western leg.

The axial field direction, along $\mathbf{A}$, is parallel to $d\mathbf{P}_A(t)/dt = V_{SW}\widehat{\mathbf{R}} + R\Omega\widehat{\theta}$, thus

$$\widehat{\mathbf{A}} = \frac{(V_{SW}\widehat{\mathbf{R}} + R\Omega\widehat{\theta})}{\sqrt{V_{SW}^2 + (R\Omega)^2}}. \tag{2}$$

The vector $\mathbf{N}(t)$ is taken to be perpendicular to $\mathbf{A}(t)$ in the $+\widehat{\mathbf{R}}$ direction. It is assumed that the flux rope is expanding isotropically at a constant speed V_{EX} in the directions orthogonal to its axis (*i.e.*, in the $\widehat{\mathbf{N}}$-direction). Thus the front and rear positions of the flux rope in the $R-\theta$ plane will be described by P_F and P_R, respectively, assuming negligible extension at the Sun ($t = 0$):

$$\mathbf{P}_F(t) = \mathbf{P}_A(t) + t\,V_{EX}\widehat{\mathbf{N}},$$
$$\mathbf{P}_R(t) = \mathbf{P}_A(t) - t\,V_{EX}\widehat{\mathbf{N}}. \tag{3}$$

These are shown as dashed black lines in Figure 1. A general position within the flux rope in the $R-\theta$ plane, $\mathbf{P}$, can thus be described by the parameter t, which effectively describes the distance along the axis, and a parameter r, which is the normalised distance from the

Figure 2 A sketch of the flux rope model used in this study. In curvilinear coordinates, the axial field is a straight line. Expansion has been ignored, assuming ds to be small. β is defined as the angle the magnetic field makes with the $R-\theta$ plane, equal to the $s-\rho$ plane.
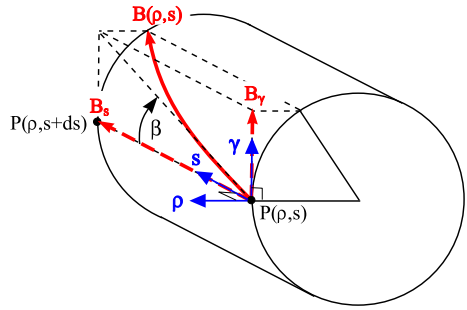
axis ($r = 0$) to the flux rope edge ($r = 1$). More precisely, we set the curvilinear abscissa $s = Vt$ along the flux rope axis (where V could be taken equal to V_{SW}, while we emphasise again that we are not describing the solar wind field). We also set the cross-sectional radius $\rho = rt V_{\text{EX}}$ of a point at a relative distance r from the axis.

The isotropic expansion of the flux rope cross section with s and the conservation of the axial flux imply that the axial magnetic field decreases with s as

$$B_{\text{A}}(s) = \frac{B_0(s = 1)}{s^2}. \tag{4}$$

The cross-sectional expansion also implies a component of the magnetic field, B_ρ, is orthogonal to the local axis direction. Since ρ increases linearly with s,

$$B_\rho(s) = B_{\text{A}}(s)\rho/s. \tag{5}$$

Next, the field profile in the cross section is set in a self-similar form:

$$B_{\text{A}}(\rho, s) = f(\rho/s)/s^2, \tag{6}$$

$$B_\rho(\rho, s) = f(\rho/s)\rho/s^3, \tag{7}$$

where f is any smooth function of ρ/s. In the local cylindrical coordinate system (ρ, γ, s), so neglecting the curvature of the axis, Equations (6) and (7) describe a generic magnetic field, invariant in γ, and satisfying $\nabla \cdot \mathbf{B} = 0$. Assuming that the axial magnetic field varies with ρ in the same manner as a linear FFFR, $f(\rho/s) = B_0(s = 1)V^2 J_0(\alpha r)$, where J_0 is the Bessel function of the zeroth order. As $\alpha r = 2.408$ corresponds to a vanishing axial field, this is typically taken as the outer edge of the flux rope when modelling MCs. Thus $r = 1$ corresponds to the outer boundary of the flux rope, and α is fixed at 2.408. In this case, Equations (6) and (7) can be rewritten as

$$B_{\text{A}}(r, t) = B_0(t = 1) J_0(\alpha r)/t^2, \tag{8}$$

$$B_\rho(r, t) = B_0(t = 1) J_0(\alpha r) r V_{\text{EX}}/(V t^2). \tag{9}$$

The flux rope nature of the field means that the magnetic field at $\mathbf{P}(\rho, s)$ makes an angle β out of the $R-\theta$ plane, as shown in Figure 2. This poloidal component of the flux rope magnetic field can be expressed as

$$B_\gamma(r, t) = H B_0(t = 1) J_1(\alpha r)/t^2, \tag{10}$$

where H is the handedness of the flux rope magnetic field about the axis (either $+1$ or -1) and J_1 is the Bessel function of the first order. As B_γ is independent of γ, $\nabla \cdot \mathbf{B} = 0$ is still satisfied if the bending of the axis is ignored.

Combining Equations (8), (7) and (10) yields the following magnetic field vector in the $R-\theta$ plane:

$$\mathbf{B}(r,t) = \frac{B_0(t=1)}{t^2}\left[J_0(\alpha r)\widehat{\mathbf{A}} + HJ_1(\alpha r)\widehat{\mathbf{Z}} + \frac{rV_{\text{EX}}}{V}J_0(\alpha r)\widehat{\mathbf{N}}\right]. \tag{11}$$

Thus locally (and instantaneously), $\mathbf{B}$ corresponds to a linear force-free field with a moderate divergence of the cross section. However, the direction of the axis, $\widehat{\mathbf{A}}$, and the flux rope radius are both functions of t, which controls the distance along the axis ($s = Vt$), resulting in the non-force-free magnetic field configuration shown in Figure 2. Bending an FFFR axis would result in a stronger field strength on the concave side compared to the convex side. The expansion of the cross section would result in the creation of a magnetic torque, which will tend to redistribute the twist along the flux rope. Both effects are not taken into account in the simple analytical expression of Equation (11). However, as the curvature radius of the axis, R_{c}, and the expansion scale length of the cross section, Vt, are both assumed to be large compared to the flux rope radius, $V_{\text{EX}}t$, the non-force-free terms are expected to be small (of the order of $V_{\text{EX}}t/R_{\text{c}}$ and V_{EX}/V, respectively). Thus the non-force-free aspect of Equation (11) is only expected to introduce a small deviation of $\mathbf{B}$ compared to the corresponding force-free field. Indeed, for this study we only need an approximate magnetic field for a local section of the flux rope, and not a global coherent model of it.

The top panel of Figure 1 shows magnetic field lines corresponding to $r = 0$, 0.3, 0.6 and 0.9 as black, green, blue and red lines, respectively. The bottom panel shows the projection onto the $R-\theta$ plane, which may be considered equivalent to the ecliptic plane in this study. As will be demonstrated in Section 3.1, a 'cut' through the curved flux rope, approximating a spacecraft trajectory through the flux rope, will generally not be a line of constant t. Thus the variation in the $\widehat{\mathbf{A}}$ direction will result in a non-zero $\widehat{\mathbf{N}}$ component in any stationary coordinate system.

3. Results

3.1. Model Time Series

Synthetic time series approximating spacecraft encounters with a curved flux rope are generated by taking radial cuts through the model magnetic field structure. Although this method ignores the effect of time evolution of the flux rope (most notably expansion) as it passes over the stationary spacecraft, in most circumstances such effects tend to be small (Owens, Merkin, and Riley, 2006).

The top panels of Figure 3 show two flux ropes, a force-free structure with a straight axis (black) and a curved flux rope (red). The diagrams are drawn in the $R-\theta$ plane. All spacecraft encounters are considered in the plane which contains the axial magnetic field, which can be considered the $X-Y$ (GSE) plane. Note that the spacecraft encountering the flux rope axis in this way is a special case. However, the errors introduced by the spacecraft passing some distance from the axis (*i.e.*, a non-zero impact factor) have been considered elsewhere (*e.g.*, Gulisano *et al.*, 2007). Here, we consider solely the effect of axial curvature and cross-sectional expansion on MC reconstruction techniques.

Flux rope axes are shown as the solid lines in Figure 3, while the boundaries of the flux ropes are shown as dashed lines. Both flux ropes have an axial field magnitude at 1 AU of 20 nT and a negative magnetic helicity. The large black arrows show spacecraft trajectories through the flux ropes. Both straight and curved flux ropes have the same duration and
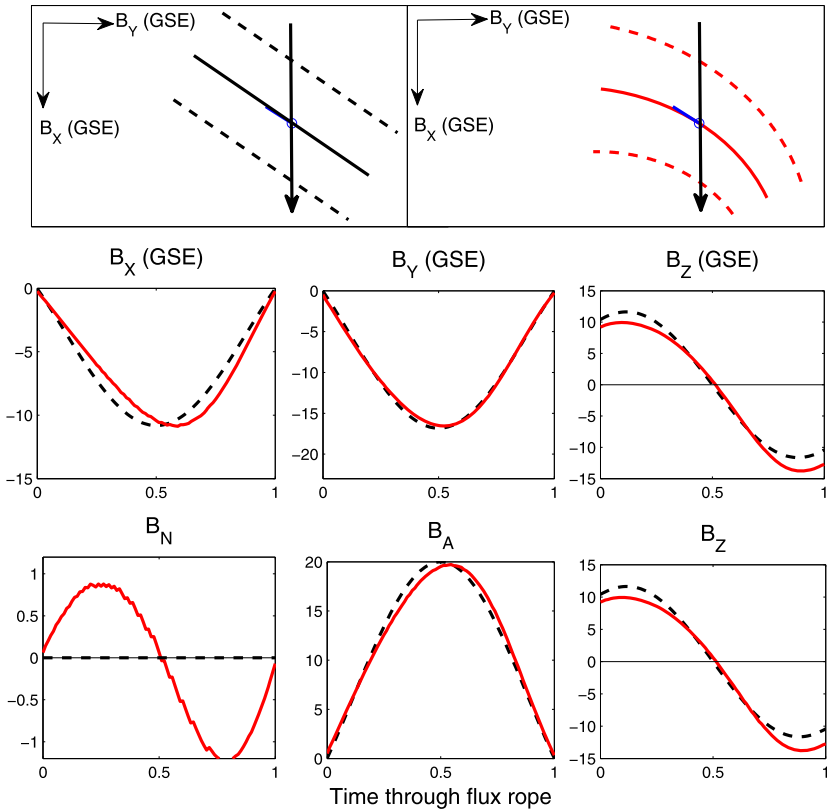
Figure 3 Top panels: Axes (solid lines) and boundaries (dashed lines) of straight-axis force-free (black) and curved (red) flux ropes in the $X-Y$ (GSE) plane. The large black arrows represent spacecraft trajectories through the structures, which have the same local axis orientation at the point of spacecraft intercept. Middle panels: Magnetic field vectors in GSE coordinates as simulated along the spacecraft trajectory in function of a normalised coordinate (0: entrance, 1: exit). Bottom panels: Magnetic field vectors in the flux rope coordinate system.

local axis orientation, namely $[-0.537, -0.844, 0]$ in geocentric solar ecliptic (GSE) coordinates. A 'time series' corresponding to this trajectory can be obtained by taking a radial cut, in this particular case along a line of constant θ. The middle and bottom panels show the magnetic field vectors in GSE and local flux rope coordinates, respectively. For this encounter, the straight and curved flux rope time series are very similar. The B_N component shows the most systematic deviation, with a bipolar signature in the curved flux rope time series, but this is small in magnitude compared with the B_A and B_Z components and for real spacecraft data would probably be lost in the noise.

In order to quantify the ability of cylindrical techniques to reconstruct the properties of a curved flux rope, we compute ϵ, the angular error between the true and reconstructed local flux rope axis orientations. Applying minimum variance analysis (MVA) to the CFR **B** time series results in an axis orientation of $[-0.544, -0.838, -0.028]$ in GSE coordinates and hence an angular error of $\epsilon_{MVA} = 1.7°$. Fitting a force-free flux rope (FFFR) model to the CFR **B** time series gives an axis of $[-0.539, -0.842, 0.004]$ and $\epsilon_{FFFR} = 0.3°$. Thus, in this instance, the effect of axial curvature and cross-sectional expansion on the ability of
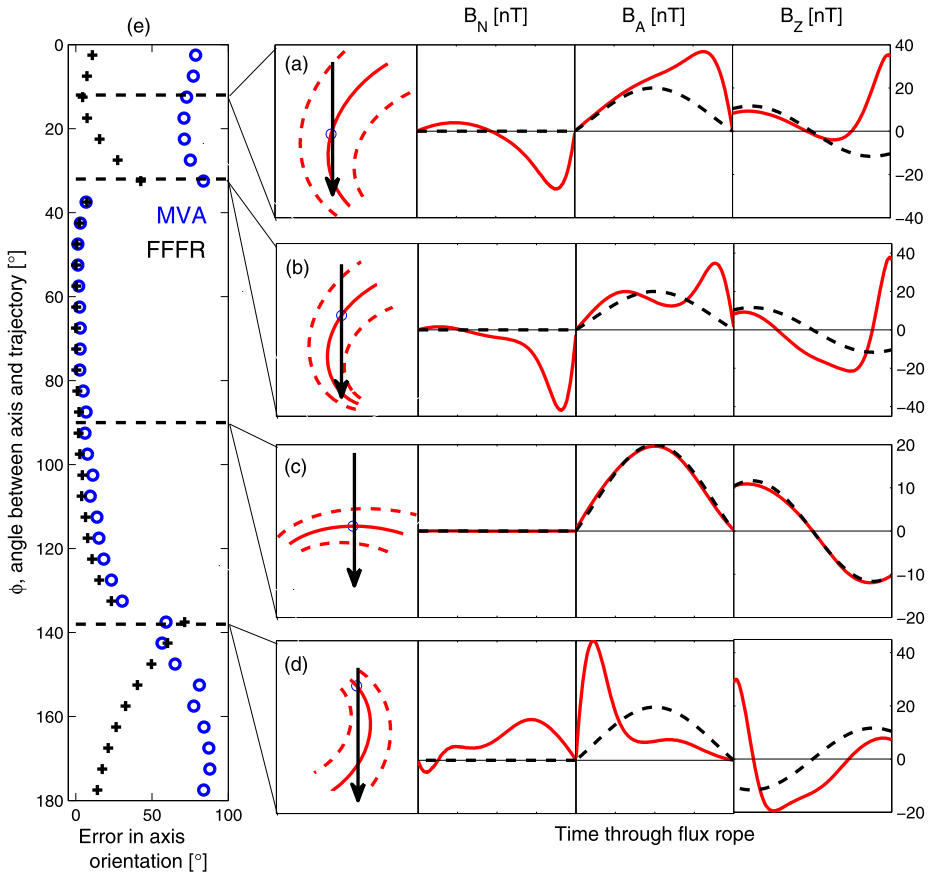
Figure 4 Effect of ϕ, the angle between the spacecraft trajectory and axis, on MC reconstruction. The black arrows in panels a–d show four different spacecraft trajectories through the curved flux rope. Next to each trajectory is the curved (red) and force-free (black dashed) flux rope time series (in the local flux rope coordinate system defined by the model with A along the flux rope axis and N normal to it). Panel e shows the error in the axis estimation from MVA (black) and FFFR fitting (blue) with ϕ.

cylindrical techniques to reconstruct the local axis orientation is very small (but could be significant depending on the application, as shown below).

3.2. Local Axis Orientation

In this section, the variation of ϵ with ϕ, the angle between the local flux rope axis angle and the spacecraft trajectory (*i.e.*, the radial direction), is investigated.

Panel c of Figure 4 shows a flux rope encounter which results in a local axis orientation, the red solid line, perpendicular to the radial direction, the black solid arrow. This results in the red magnetic field time series shown in the right-hand panels. B_N, B_A and B_Z are the magnetic field components in the local flux rope coordinates. The black dashed lines show the equivalent straight-axis flux rope time series, which are very similar to the CFR time series. In a similar result to the example shown in the previous section, this results in a $\approx 6°$ ($\approx 5°$) error in the local axis orientation reconstructed using minimum variance analysis (FFFR fitting).

Panel e shows how ϵ, the error in the reconstructed axis orientation varies, with ϕ, the angle of the spacecraft trajectory to the axis. For the range $\approx 35° \lesssim \phi \lesssim 140°$, this error is typically $\approx 5 - 20°$ for both MVA and FFFR modelling, although FFFR systematically gives a slightly more accurate reconstruction. However, outside of this range, ϵ increases rapidly. Panels a, b and d clearly show the reason; the curvature of the axis allows the spacecraft to encounter the axis twice before exiting the flux rope structure. In these circumstances, FFFR fitting performs much better than MVA, although the error in the axis orientation can still reach $\approx 75°$. We note that encounters b and d produce magnetic field time series which could potentially be interpreted as spacecraft trajectories through two flux ropes of the same helicity but different orientations. This has been noted and modelled in spacecraft observations (Rees and Forsyth, 2004). Consequently, an observer might choose to analyse only part of a time series. The implications of this are investigated in the next section. Also of interest is encounter (a), in which the spacecraft is approximately along the axis direction. In this instance, the axis orientation determined by FFFR fitting is surprisingly accurate, although MVA does not perform well.

3.3. 'Double Flux Rope' Encounters

In this section we investigate the error in axis orientation from cylindrical models when a MC exhibits an apparent 'double flux rope' signature. Figure 5 shows an example. In the leftmost panel, the solid red line shows the axial field of the flux rope, the dashed red lines show the boundaries of the flux rope, and the black line shows the spacecraft trajectory. The spacecraft encounters the axis at two points, labelled A and B. The time series, in GSE coordinates and flux rope coordinates (using the axis orientation at A), are also shown. Determination of the boundary between the two flux rope encounters is somewhat subjective. We use the local maximum in B_X GSE (which is equivalent to the local minimum in B_A because B_Y is small) to set the boundary at 0.65 of the time through the entire structure, shown as the vertical black dashed lines. Varying the precise position of this boundary does not qualitatively affect the results below.

At 'A', the local axis orientation is $[-0.887, -0.462, 0.000]$ in GSE coordinates, whereas it is $[-0.860, 0.500, 0]$ at 'B'. Using the magnetic field time series over the entire CFR encounter, MVA gives an axis orientation of $[-0.721, 0.525, -0.453]$, $67°$ from the orientation at A, and $27.5°$ from the orientation at B. FFFR fitting gives $[-0.823, -0.130, -0.539]$, $37°$ from the orientation at A and $49°$ from the orientation at B.

Using only data from the interval designated FR_A, MVA gives an axis orientation of $[-0.835, -0.509, 0.211]$, only $13°$ from the true local axis orientation at A. For the interval FR_B, MVA gives $[-0.839, 0.438, -0.324]$, $19°$ from the true orientation at B. FFFR fitting to FR_A gives $[-0.581, -0.801, -0.141]$, $28°$ from the true orientation. Similarly, FFFR fits to FR_B give $[0.186, 0.983, 0]$, $39°$ from the true orientation.

The poor reconstruction of the axis orientation with the FFFR model is the result of unequal sampling of the magnetic flux either side of the axis encounters. For example, for the interval FR_A the spacecraft samples magnetic flux which maps to $0 < r < 1$ during its approach to the axis at A, but after crossing the axial field it only sees $-0.55 < r < 0$ before entering region FR_B, where it begins to approach the axis again. As FFFR models are constrained to have an axis encounter (or point of closest approach to the axis) midway through the time series, it is unsurprising that ϵ is large. One means to mitigate this effect is to only fit the 'core' field with an FFFR model, so as to sample approximately equal amounts of the structure either side of the axis encounter. For encounter A, this would require estimating the
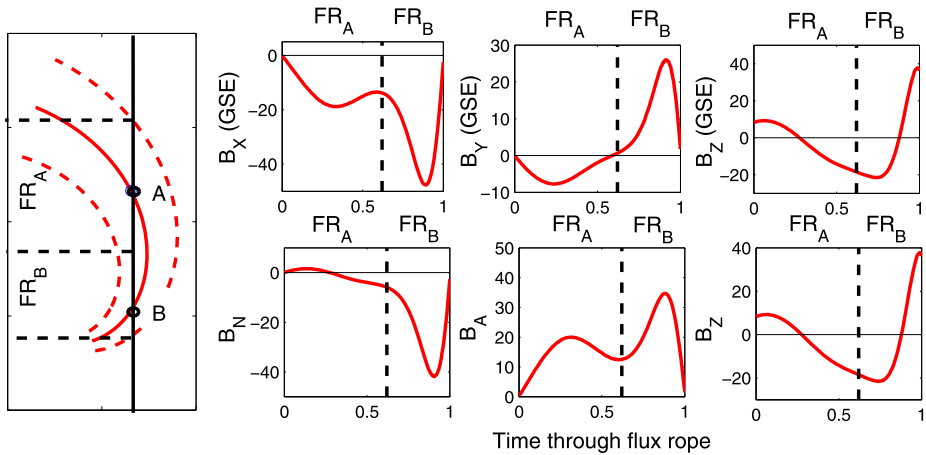
Figure 5 An example of an encounter with a curved flux rope which results in a magnetic field time series which could be interpreted (and modelled) as a 'double flux rope'. The three top right panels are in GSE coordinates, while the three bottom right panels are in flux rope coordinates at A. Choosing the boundary between the two axis encounters, FR_A and FR_B, is somewhat subjective.

section of FR_A for which $-0.55 < r < 0.55$, which would translate to roughly 0.25 to 0.65 of the time through the whole structure. It would then be necessary to relax the $\alpha = 2.408$ assumption, as the edge of this core flux rope would no longer correspond to a completely poloidal field. In practice, this approach would have a number of limitations, particularly the lack of systematic means to select the core flux rope from the time series, α as an extra free parameter of the fit, and the reduction in the amount of data used in the reconstruction. It is probably simpler and more reliable to use MVA for the purpose of double flux rope analysis.

4. Discussion and Conclusions

This paper describes a flux rope model for magnetic clouds (MCs) in which cylindrical symmetry is relaxed by allowing a curved axial field. Additionally, it further relaxes some of the constraints of spheromak and toroidal models by allowing both the axial curvature and the cross-sectional extent of the flux rope to vary along the length of the axis. While this model may or may not accurately describe the global structure of MCs, it does allow us to investigate the effect of axial curvature and cross-sectional expansion on flux rope reconstruction techniques. Other sources of error to MC reconstruction techniques are not considered here. In particular, we only consider spacecraft encounters with the axis of the flux rope (*i.e.*, the impact parameter is set to zero), and the model has a linear force-free profile without distortion.

Radial cuts through this curved flux rope model approximate stationary spacecraft encounters with MCs. Assuming the spacecraft crosses the axis of the flux rope approximately perpendicularly, the effect of axial curvature typically introduces an error of only $\approx 5 - 10°$ into estimates of axis orientation from minimum variance analysis (MVA) or force-free flux rope (FFFR) fitting. In general, FFFR fitting reproduces the axis orientation slightly more accurately than MVA (for this test model based on a linear force-free profile). However, when the local magnetic flux rope axis is within $\approx 45°$ of the radial direction (*i.e.*, the space-craft trajectory through the flux rope), the error in MVA/FFFR reconstruction of the axis

orientation can increase to $\approx 90°$. This is the result of the spacecraft encountering the axis twice before exiting the flux rope structure, causing the magnetic field time series to deviate significantly from that of an encounter with a force-free configuration.

We note that in the limiting cases where the spacecraft skirts the trailing edge of the flux rope before returning to the axis, the magnetic field time series looks much like an encounter with two flux ropes of the same helicity but different orientations, as is sometimes observed (Rees and Forsyth, 2004; Marubashi and Lepping, 2007). Consequently, an observer might choose to fit the two apparent flux ropes independently. Attempting such a procedure, we found that MVA works reasonably well, determining the local axis orientation within $\approx 20 - 30°$ at both axis intersections. However, FFFR fitting produces errors about twice. This is the result of uneven sampling of magnetic flux either side of the axis encounters. We suggest a method to mitigate this effect, but the simplest solution may just be to use MVA for analysis of double flux ropes.

References

Bothmer, V., Schwenn, R.: 1998, The structure and origin of magnetic clouds in the solar wind. *Ann. Geophys.* **16**, 1 – 24.

Burlaga, L.F.: 1988, Magnetic clouds: Constant alpha force-free configurations. *J. Geophys. Res.* **93**, 7217 – 7224.

Burlaga, L.F., Sittler, E., Mariani, F., Schwenn, R.: 1981, Magnetic loop behind an interplanetary shock: Voyager, Helios, and IMP 8 observations. *J. Geophys. Res.* **86**, 6673 – 6684.

Cane, H.V., Richardson, I.G.: 2003, Interplanetary coronal mass ejections in the near-Earth solar wind during 1996 – 2002. *J. Geophys. Res.* **108**, 1156. doi:10.1029/2002JA009817.

Cremades, H., Bothmer, V.: 2004, On the three-dimensional configuration of coronal mass ejections. *Astron. Astrophys.* **422**, 307 – 322. doi:10.1051/0004-6361:20035776.

Dungey, J.W.: 1961, Interplanetary magnetic field and the auroral zones. *Phys. Rev. Lett.* **6**, 47.

Farrugia, C.J., Osherovich, V.A., Burlaga, L.F.: 1995, Magnetic flux rope versus the spheromak as models for interplanetary magnetic clouds. *J. Geophys. Res.* **100**, 12293. doi:10.1029/95JA00272.

Gosling, J.T.: 1993, The solar flare myth. *J. Geophys. Res.* **98**, 18937 – 18950. doi:10.1029/93JA01896.

Gosling, J.T., Baker, D.N., Bame, S.J., Feldman, W.C., Zwickl, R.D.: 1987, Bidirectional solar wind electron heat flux events. *J. Geophys. Res.* **92**, 8519 – 8535.

Gulisano, A.M., Dasso, S., Mandrini, C.H., Démoulin, P.: 2007, Estimation of the bias of the minimum variance technique in the determination of magnetic clouds global quantities and orientation. *Adv. Space Res.* **40**, 1881 – 1890. doi:10.1016/j.asr.2007.09.001.

Hidalgo, M.A., Cid, C., Vinas, A.F., Sequeiros, J.: 2002, A non-force-free approach to the topology of magnetic clouds. *J. Geophys. Res.* **107**, 1002 – 1009. doi:10.1029/2001JA900100.

Hu, Q., Sonnerup, B.U.O.: 2001, Reconstruction of magnetic flux ropes in the solar wind. *Geophys. Res. Lett.* **28**, 1443.

Hundhausen, A.J.: 1993, Sizes and locations of coronal mass ejections – SMM observations from 1980 and 1984 – 1989. *J. Geophys. Res.* **98**, 13177 – 13200.

Klein, L.W., Burlaga, L.F.: 1982, Interplanetary magnetic clouds at 1 AU. *J. Geophys. Res.* **87**, 613 – 624.

Lavraud, B., Borovsky, J.E.: 2008, Altered solar wind-magnetosphere interaction at low Mach numbers: Coronal mass ejections. *J. Geophys. Res.* **113**, A00B08. doi:10.1029/2008JA013192.

Lavraud, B., Owens, M.J., Rouillard, A.P.: 2011, In situ signatures of interchange reconnection between magnetic clouds and open magnetic fields: A mechanism for the erosion of polar coronal holes? *Solar Phys.* **270**, 285 – 296. doi:10.1007/s11207-011-9717-6.

Lepping, R.P., Jones, J.A., Burlaga, L.F.: 1990, Magnetic field structure of interplanetary clouds at 1 AU. *J. Geophys. Res.* **95**, 11957 – 11965.

Lynch, B.J., Gruesbeck, J.R., Zurbuchen, T.H., Antiochos, S.K.: 2005, Solar cycle dependent helicity transport by magnetic clouds. *J. Geophys. Res.* **110**, A08107. doi:10.1029/2005JA011137.

Marubashi, K., Lepping, R.P.: 2007, Long-duration magnetic clouds: A comparison of analyses using torus- and cylinder-shaped flux rope models. *Ann. Geophys.* **25**, 2453 – 2477. doi:10.5194/angeo-25-2453-2007.

Mulligan, T., Russell, C.T.: 2001, Mulitspacecraft modeling of the flux rope structure of interplanetary coronal mass ejections: Cylindrical symmetric versus nonsymmetric topologies. *J. Geophys. Res.* **106**, 10581 – 10596.

Owens, M.J.: 2008, Combining remote and in situ observations of coronal mass ejections to better constrain magnetic cloud reconstruction. *J. Geophys. Res.* **113**, A12102. doi:10.1029/2008JA013589.

Owens, M.J., Cargill, P.J.: 2004, Non-radial solar wind flows induced by the motion of interplanetary coronal mass ejections. *Ann. Geophys.* **22**, 4395 – 4397.

Owens, M.J., Crooker, N.U., Horbury, T.S.: 2009, The expected imprint of flux rope geometry on suprathermal electrons in magnetic clouds. *Ann. Geophys.* **27**, 4057 – 4067. doi:10.5194/angeo-27-4057-2009.

Owens, M.J., Merkin, V.G., Riley, P.: 2006, A kinematically distorted flux rope model for magnetic clouds. *J. Geophys. Res.* **111**, A03104. doi:10.1029/2005JA011460.

Owens, M.J., Schwadron, N.A., Crooker, N.U., Hughes, W.J., Spence, H.E.: 2007, Role of coronal mass ejections in the heliospheric Hale cycle. *Geophys. Res. Lett.* **34**, L06104. doi:10.1029/2006GL028795.

Rees, A., Forsyth, R.J.: 2004, Two examples of magnetic clouds with double rotations observed by the Ulysses spacecraft. *Geophys. Res. Lett.* **31**, L06804. doi:10.1029/2003GL018330.

Riley, P., Crooker, N.U.: 2004, Kinematic treatment of CME evolution in the solar wind. *Astrophys. J.* **600**, 1035 – 1042.

Riley, P., Linker, J.A., Lionello, R., Mikic, Z., Odstrcil, D., Hidalgo, M.A., Hu, Q., Lepping, R.P., Lynch, B.J., Rees, A.: 2004, Fitting flux-ropes to a global MHD solution: A comparison of techniques. *J. Atmos. Solar-Terr. Phys.* **66**, 1321 – 1332.

Romashets, E., Vandas, M.: 2009, Linear force-free field of a toroidal symmetry. *Astron. Astrophys.* **499**, 17 – 20. doi:10.1051/0004-6361/200911701.

Russell, C.T., Mulligan, T.: 2002, On the magnetosheath thicknesses of interplanetary coronal mass ejections. *Planet. Space Sci.* **50**, 527 – 534.

Savani, N.P., Owens, M.J., Rouillard, A.P., Forsyth, R.J., Davies, J.A.: 2010, Observational evidence of a coronal mass ejection distortion directly attributable to a structured solar wind. *Astrophys. J. Lett.* **714**, L128 – L132. doi:10.1088/2041-8205/714/1/L128.

Sonnerup, B.U.O., Cahill, L.J.: 1967, Magnetopause structure and attitude from Explorer 12 observations. *J. Geophys. Res.* **72**, 171.

Vandas, M., Romashets, E.P.: 2003, A force-free field with constant alpha in an oblate cylinder: A generalization of the Lundquist solution. *Astron. Astrophys.* **398**, 801 – 807. doi:10.1051/0004-6361:20021691.

Vandas, M., Fischer, S., Geranios, A.: 1991, Spherical and cylindrical models of magnetized plasma clouds and their comparison with spacecraft data. *Planet. Space Sci.* **39**, 1147 – 1154. doi:10.1016/0032-0633(91)90166-8.

Vandas, M., Fischer, S., Dryer, M., Smith, Z., Detman, T.: 1998, Propagation of a spheromak 2. Three-dimensional structure of a spheromak. *J. Geophys. Res.* **103**, 23717 – 23726. doi:10.1029/98JA01902.

Wang, Y., Zhou, G., Ye, P., Wang, S., Wang, J.: 2006, A study of the orientation of interplanetary magnetic clouds and solar filaments. *Astrophys. J.* **651**, 1245 – 1255. doi:10.1086/507668.

Wimmer-Schweingruber, R.F., Crooker, N.U., Balogh, A., Bothmer, V., Forsyth, R.J., Gazis, P., Gosling, J.T., Horbury, T., Kilchmann, A., Richardson, I.G., Riley, P., Rodriguez, L., von Steiger, R., Wurz, P., Zurbuchen, T.H.: 2006, Understanding interplanetary coronal mass ejection signatures. *Space Sci. Rev.* **123**, 177 – 216. doi:10.1007/s11214-006-9017-x.

Yamamoto, T.T., Kataoka, R., Inoue, S.: 2010, Helical lengths of magnetic clouds from the magnetic flux conservation. *Astrophys. J.* **710**, 456 – 461. doi:10.1088/0004-637X/710/1/456.